Mathematical Modeling of Fuel Cell Cathode with High Temperature

S. Srimongkol, S. Rattanamongkonkul, A. Pakapongpun, S. Pleumpreedaporn, D. Poltem

***Abstract*—**In this paper, the study of fuel cells is briefly reviewed. To reduce the cost, the mathematical modeling is an essential tool to study the behavior of fuel cell. Various mathematical models are used to investigate the performance of various fuel cells. Thus, the investigation of mathematical modeling of fuel cell cathode is crucial. The model is coupled the equations for electron transport, the Maxwell-Stefan equation, and Darcy's law for flow in porous media. The numerical results is used the high temperature, $1273K$. The numerical results of the fuel cell cathode are examined using finite element method. The mass fraction of oxygen, velocity field, and electric potential are presented. It is showed that the mathematical model is able to model the high temperature fuel cell cathode.

***Keywords*—**Electron transport, Mass transport, Maxwell-Stefan equations, Fuel cell cathode, Mathematical modeling, Numerical method.

I. Introduction

In recent years, there has been number of publications in the development of fuel cells. Due to the limit of fossil fuel, petroleum products are not going to supply the increasing global demand. Pollution and global warming are also the crutial problems. Transportation and fuel combustion are the main sources of air pollution [2]. Therefore, the alternative renewable energy technologies have been main impetus. Biofuels, wind power, solar energy and nuclear energy are examples of alternative renewable energy [3], [18]. Fuel cell is the low level emissions which is a possible solution of this problem [29], [19], [4], [23], [6], [7].

Fuel cell is a device which converts the energy from fuel to electrical power and produces water as its byproduct. The fuel cell system is flexibility in sizing and the operation is quiet. There are six main types of fuel cell: alkaline fuel cell (AFC), phosphoric acid fuel cell (PAFC), molten carbonate fuel cell (MCFC), polymer electrolyte membrane fuel cell (PEMFC), direct methanol fuel cell (DMFC), and solid oxide fuel cell (SOFC) [12], [17]. SOFC is the highest operating temperature as shown in TABLE I. Advantages of high operating temperature are high energy conversion efficiency, flexibility of fuels, high temperature exhaust gas. Disadvantages are thermal fatigue failure of the fuel cell material and the thermal stress which is induced by cell temperature fluctuations. During the last two decades, the number of SOFCs research papers has been dramatically increasing [17], [14]. Tubular and planar SOFCs are the most popular designs [23], [14], [27], [10], [30], [5], [28].

S. Srimongkol is with the Department of Mathematics, Faculty of Science, Burapha University, and Centre of Excellence in Mathematics, PERDO, CHE, THAILAND e-mail: sineenart@buu.ac.th.

S. Rattanamongkonkul is with the Department of Mathematics, Faculty of Science, Burapha University, and Centre of Excellence in Mathematics, PERDO, CHE, THAILAND e-mail: sahattay@buu.ac.th.

A. Pakapongpun is with the Department of Mathematics, Faculty of Science, Burapha University, and Centre of Excellence in Mathematics, PERDO, CHE, THAILAND e-mail: apisit.buu@gmail.com.

D. Poltem is with the Department of Mathematics, Faculty of Science, Burapha University, and Centre of Excellence in Mathematics, PERDO, CHE, THAILAND e-mail: duangkamolp@buu.ac.th.

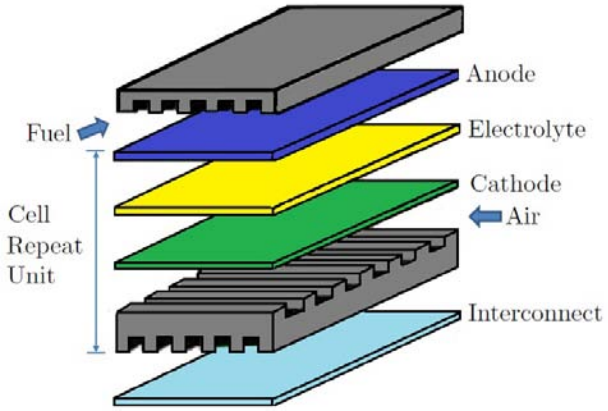

Fig. 1. Planar SOFC structure.

TABLE I
Approximate operating temperature of fuel cells.

Fuel Cell	Operating Temperature (K)	Efficiency (%)
AFC	323–373	50–70
PAFC	448–493	40–45
MCFC	873–923	50–60
PEMFC	333–373	40–50
DMFC	323–393	25–40
SOFC	923–1273	50–60

SOFCs are used for mid- to large- scale applications. Currently, most types of fuel cells are considered for automobiles and stationary power plants. Normally, the physical property of the fuel cell consists of an electrolyte layer in contact with a porous anode and a cathode on either side. The configuration of single cell planar SOFCs is shown in Fig. 1. The SOFCs electrolyte is a layer of ceramic material with high-temperature endurable porous media electrodes. A mixture of zirconium oxide, calcium oxide forms a crystal lattice, and other oxide combinations have also been used as SOFCs electrolyte.

SOFCs are flexible for the use of fuels. Several hydrocarbons and carbon monoxide (CO) can be used as fuels. When using hydrogen fuel, the chemical reactions of the SOFC [17] are as follow.

At anode side of SOFCs, reaction of the input hydrogen and

with oxygen ion produces water and electron,

$$H^2 + 2O^{2-} \rightarrow 2H_2O + 4e^-,$$

at cathode,

$$O_2 + 4e^- \rightarrow 2O^{2-}.$$

The cell reaction is

$$O_2 + 2H_2 \rightarrow 2H_2O.$$

In 1838, the basic principle of the fuel cell was found by Friderich Schnbein. In 1950, Francis Bacon demonstrated the first 5kW alkalinahoe fuel cell. In 1970, 12 kW alkaline fuel cell was developed. In the mid-1960s, the fuel cell research work was focused on the development of various fuel cells for stationary powers and transportation [12]. Yakabe et al. [33] constructed a three-dimensional mathematical model for a planar SOFC. In the single-unit model of SOFCs, the concentrations of the chemical species, the temperature distribution, the potential distribution, and the current density were computed by using governing equations which consist of the mass and momentum conservation, the enthalpy conservation equation, the mass balance of the total gas, and enthalpy balance. The numerical results showed that the stream reforming generated internal stresses about $10\ MPa$ in an electrolyte. They also found that the co-flow pattern reduced the internal stresses.

Hussain and Dincer [16] had developed a mathematical model to predict the performance of planar solid oxide fuel cell. Their model can apply both pure hydrogen and reformate composition such as water, methane, carbon dioxide as a fuel. By using finite-volume method, they found that the anode concentration overpotential in an anode-supported SOFC is about four orders of magnitude smaller than the anode ohmic overpotential at the reaction zone layers.

The performance of hybrid power systems, solid oxide fuel cell and gas turbine, is shown that the system with internal reforming gives better efficiency and power capacity than the system with external reforming under the same constraints. Air bypass after the compressor and additional fuel supply to the turbine side were used to examine the effect of matching between the fuel cell temperature and the turbine inlet temperature on the hybrid system performance. When the cell temperature difference becomes smaller, the hybrid system performance degrades [35].

Ho et al. [14] presented a numerical model for a planar SOFC with mixed ionic-electronic conducting electrodes. In the composite electrodes and through the electrolyte membrane used an algorithm for Fickian diffusion in the commercial package Star-CD. The model describes the conservation of mass, momentum, energy, and chemical and electrochemical precesses. The results show the concentration of chemical species and the distributions of temperature and current density in an anode-supported SOFC with direct internal reforming.

A mathematical model for a planar solid oxide fuel cell coupled electrochemical kinetics, gas dynamics and transport of energy and species. The analysis has been performed by the use of an program which used to understand the effects of various parameters on the performance of SOFCs. Polarization curve, velocity and temperature fields, species concentration and current distribution in the fuel cell depending on fuel cell temperatures and electrolyte materials were predicted using the model. Operating temperatures of the fuel cell which are 773, 873, and 1073 K were used in the investigation. The result was shown that the anode-supported solid oxide fuel cells with YSZ electrolyte obtained a high power density in the higher current density than the YSZ electrolyte-supported solid oxide fuel cells [25].

A PEMFC is also a clean energy which is fed with hydrogen and oxygen or air. Behavior of PEMFCs depends on a number of parameters such as temperature, pressure and humidity [20]. Qianpu Wang et al. [32] studied the mathematical model of PEMFC. The model can use to consider the kinetics of oxygen reduction, proton transport , the oxygen diffusion, and the dissolved oxygen diffusion with limit of oxygen diffusion control, proton conductivity control, and mixture control. Qiangu Yan and Junxiao Wu [34] used the numerical model to obtain a geometric description of the active layer. The model is based on the microstructure of the catalyst layer. The result indicates that platinum particle size, platinum loading and ionomer thickness effect local mass and charge transport in the PEMFC catalyst.

Sadiq Al-Baghdadi [19] studied fluid flow in PEMFCs to simulate stress distribution under the humidity and temperature effects. The results indicate that nonuniform stress distribution during cell operation cause cracks and pinholes in the fuel cell components. N. Akhtar, and P.J.A.M. Kerkhof [1] developed a numerical model of a PEMFC cathode with a tapered channel design to examine the dynamic behavior of liquid water transport. The level-set method using in COMSOL 3.5a, a commercial finite element method software, was used to track the liquidgas interface. The results showed that when airflow velocity is increased, water exhaust is reduced in tapering the downstream channel. There are a number of research about the use of catalysts for both the fuel oxidation at the anode and oxygen reduction at the cathode [24], [8], [26]. To reduce the costs associated with Pt cathode catalysts, non-precious metal catalysts is alternate [24].

Ni et al. [23], [22] developed mathematical model to study ammonia fed and methane fed SOFCs. Parametric analysis showed that all the overpotentials decreased with increasing temperature. Garcia-Camprubi et al. [11] showed the model and algorithm to simulate mass transfer between a channel and its electrode. By using OpenFOAM, an open source finite volume method based CFD tool, the model had been validated both planar and tubular SOFC by comparison between the experimental data and the model result.

Wang et al. [31] developed a mathematical model associated with the microfluidic fuel cell cathode operation. The model is investigated for four regions; gas channel, gas diffusion layer, catalyst layer and electrolyte microchannel. Microflow, species transport, charge transport is solved. It is found that the internal transfer resistance decreases with increasing catalyst layer porosity.

Mathematical models of fuel fed- solid oxide fuel cells are developed [9], [22], [23], [21], [15], [13]. G. Nahar, , K. Kendall [21] have formulated biodiesel as fuel for internally reforming solid oxide fuel cell. The best performance was

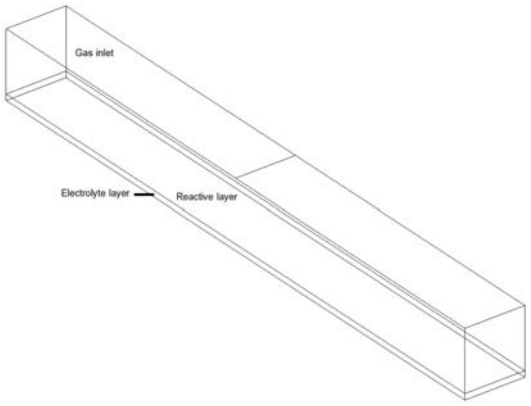

Fig. 2. Computational domain consists of reactive and electrolyte layers.

found by using 20% ethyl formulation in terms of life of the cell but 50% methyl ester formulations was the highest power density. Ta-Jen Huang, Chen-Yi Wu, Chun-Hsiu Wang [15] studied the reaction mechanism of propane internal reforming in the SOFC. They found that propane internal reforming in the SOFC is stable.

S.A. Hajimolana et al. [13] developed a dynamic model of an ammonia fed-tubular solid oxide fuel cell. Diffusion, inherent impedance, heat and mass transport, electrochemical reactions, activation and concentration polarizations of electrodes, and the ammonia decomposition reaction were taken into account. Their results indicated that the inner cell tube diameter had the strongest effect on fuel cell efficiency and the influence of cathodic porosity on fuel cell performance is higher than that of the anodic porosity.

The mathematical model in fuel cell is an important tool to study the behavior inside the fuel cell. There are numerous mathematical models for fuel cells but still have to develop for the various investigations. In this paper, the mathematical model for fuel cell cathode is presented. The high temperature is taken into account in the numerical solutions.

II. Mathematical Modeling

The mathematical model of fuel cells is a system of equations which described the behavior of the fuel cells. Various mathematical models are used to investigate the performance of fuel cells. The numerical result of the fuel cell cathode is examined using finite element method. The model is coupled the equations for electron transport, the Maxwell-Stefan equation, and Darcy's law for flow in porous media [14], [17].

A. Governing Equations

Computational domain used to study fuel cell is shown in Fig. 2. It consists of reactive and electrolyte layers. Governing equations consist of several equations. The ionic current balance in the cathode is governed by the following equation,

$$\nabla \cdot \left(\sigma_l^{eff} \nabla \phi_l\right) = -A i_{ct} \tag{1}$$

where σ_l^{eff} is the effective electrolyte conductivity (S/m), ϕ_l is the electrolyte potential (V), A is surface area, and i_{ct} is the local charge transfer current density (A/m^2). The ionic current balance in the electrolyte between cathode and cathode is

$$\nabla \cdot (\sigma_l \nabla \phi_l) = 0 \tag{2}$$

where σ_l is the conductivity of the electrolyte (S/m). The electronic charge balance in the electrode subdomain is governed by

$$\nabla \cdot \left(\sigma_s^{eff} \nabla \phi_s\right) = -A i_{ct} \tag{3}$$

where σ_s^{eff} is the effective conductivity in the solid phase (S/m), ϕ_s is the solid phase potential (V). The local charge transfer current density which is used to couple current balances and mass balances is as following

$$i_{ct} = i_0 \left[e^{\phi} - \frac{c_{O_2}}{c_{O_2,ref}} e^{\phi}\right], \tag{4}$$

$$\phi = \frac{0.5F(\phi_s - \phi_l - \Delta\phi_{eq})}{KT},$$

where $\Delta\phi_{eq}$ is the equilibrium potential difference (V), F is Faraday's constant (As/mol), K is the gas constant $(J/(mol \cdot K))$, T is the temperature (K), and c_{O_2} is the concentration of oxygen (mol/m^3)

The mass transport is given by the Maxwell-Stefan equation,

$$\frac{\partial}{\partial t}(\rho\omega_i) + \nabla \cdot (\rho \mathbf{V} \omega_i) + \nabla \cdot \mathbf{J}_i = S_{ai} \tag{5}$$

for oxygen and water in the gas phase where ω_i is the mass fraction of species i, J_i is the diffusive mass flux of species i, and S_{ai} is the additional species source. Assume that the air is saturated, the reaction produced no water vapor. The porous media is governed by the Darcy's law and mass conservation equation,

$$\mathbf{V} = -\frac{k_p}{\nu} \nabla p \tag{6}$$

$$\nabla \cdot (\rho \mathbf{V}) = S \tag{7}$$

where $\mathbf{V}$ is the velocity vector, k_p is the permeability (m^2), ν is the viscosity $(Pa \cdot s)$, p is the pressure, ρ is the density, and S is the source term. The equations (1), (3), (5), (6), and (7) used in the reactive layer and equation (2) used in the electrolyte layer.

B. Boundary Conditions

To solve the system of equations 1-6, the appropriate boundary conditions are applied. There are 12 boundaries of the domain as shown in Fig. 3. Γ_1 is the gas inlet, Γ_2 is the top near Γ_1. $\Gamma_3 - \Gamma_6$ are side boundaries of the reactive layer. $\Gamma_7 - \Gamma_{10}$ are the side boundaries of the electrolyte layer. Γ_{11} is the interface between reactive layer and electrolyte layer. Γ_{12} is the bottom of the domain.

The boundary conditions for the ionic current balances are insulating at boundaries $\Gamma_1 - \Gamma_{10}$,

$$\mathbf{n} \cdot \left(\sigma_l^{eff} \nabla \phi_l\right) = 0. \tag{8}$$

At Γ_{11} the ionic potential is

$$\phi_l = \phi_0. \tag{9}$$

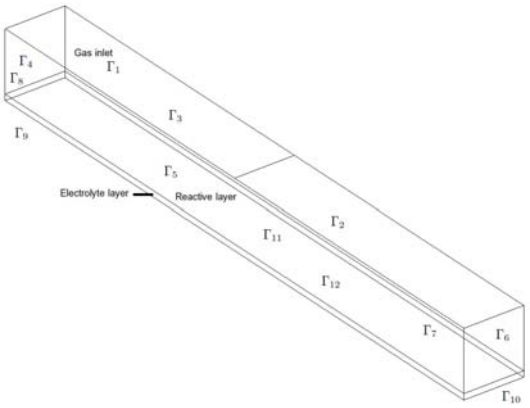

Fig. 3. Computational domain with boundary labels

The boundary condition for the electronic current balance are insulating except for the boundary Γ_2

$$\phi_s = 0. \tag{10}$$

The boundary condition for the species balances are insulating on boundaries $\Gamma_2 - \Gamma_6$, Γ_{11}

$$\mathbf{n} \cdot \mathbf{n}_i = 0 \tag{11}$$

where $\mathbf{n}_i$ is the mass flux vector for species i, and $\mathbf{n}$ is the normal vector to the boundary. The gas inlet (Γ_2) is

$$\omega_i = \omega_{i0}. \tag{12}$$

For the Darcy's law, boundary condition for all boundaries are insulating

$$\mathbf{n} \cdot \left(-\frac{k_p}{\nu} \nabla p \right) = 0 \tag{13}$$

except for Γ_1

$$\mathbf{V} = \mathbf{V}_0. \tag{14}$$

III. Numerical Results

A. High Temperature Model

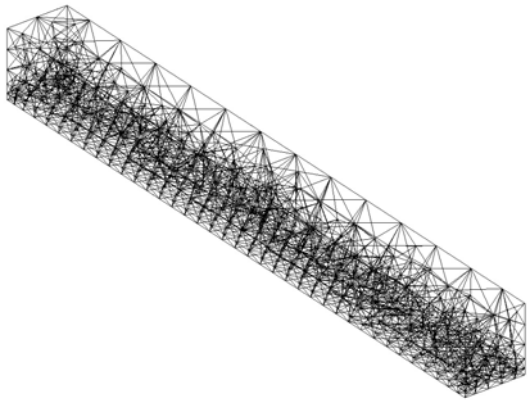

Fig. 4. Mesh of computational domain consists of 3,026 tetrahedral elements

Computational mesh generated by commercial package, COMSOL Multiphysics, consists of 3,026 tetrahedral elements is shown in Fig. 4 By using the finite element method, the numerical result is obtained. The temperature using in the numerical model is 1273 K. The three dimensional result of mass fraction of oxygen is shown in Fig. 5. The result of cross section of the mass fraction of oxygen in Fig. 6 shows that mass fraction in the reactive layer gradually increase from the left to the right side of the fuel cell. Thus, the concentration of total potential drop over the domain. The highest concentration of oxygen is on the right side of the fuel cell. The highest value of the oxygen mass fraction is 0.145.

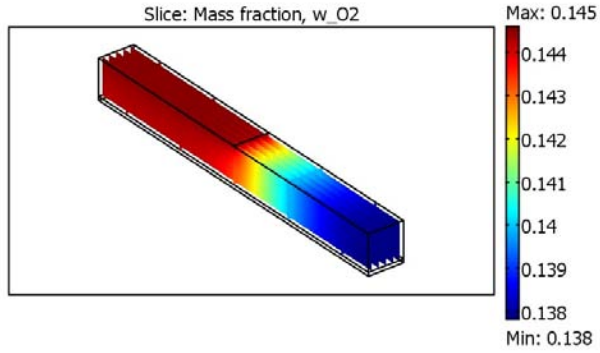

Fig. 5. Slice plot of mass fraction of oxygen at 1273 K.

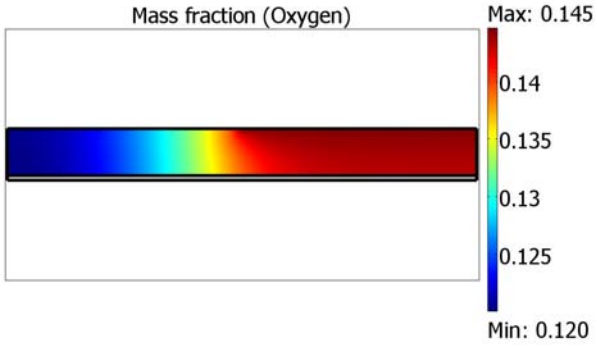

Fig. 6. Cross section of mass fraction of oxygen at 1273 K

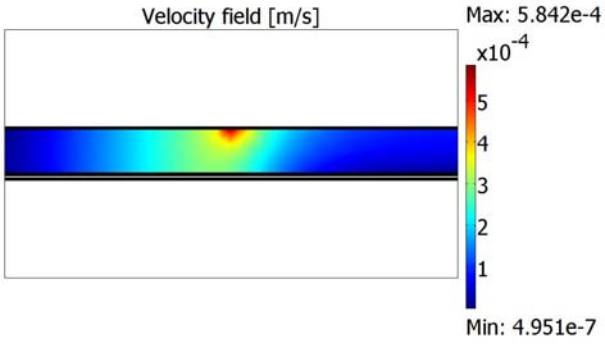

Fig. 7. Cross section plot of velocity field at 1273 K.

Fig. 7 shows the velocity in the fuel cell. The velocity peak is at the interface of the inlet. The three dimensional result of electric potential is shown in Fig. 8. Fig. 9 shows the surface plot of electric potential. The highest one is at the electrolyte

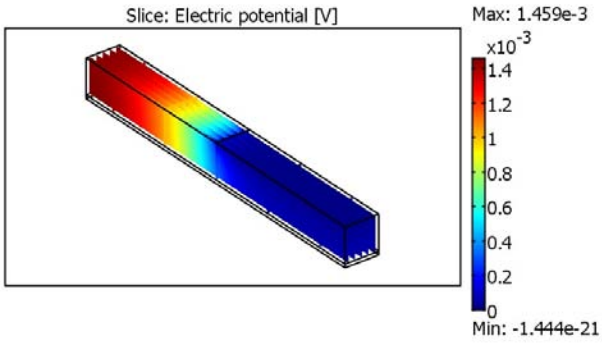

Fig. 8. Slice plot of electric potential at 1273 K.

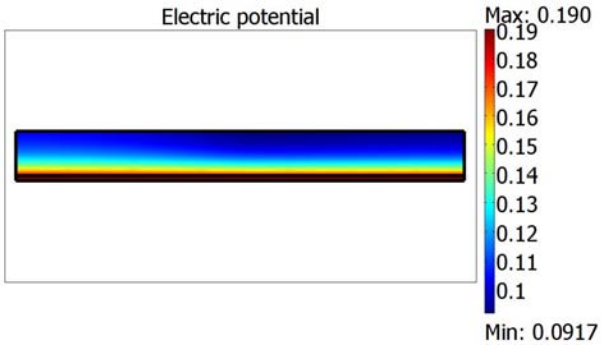

Fig. 9. Cross section plot of electric potential at 1273 K.

B. Temperature Variation

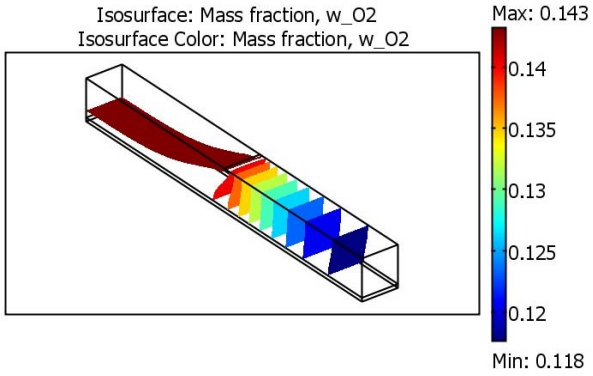

Fig. 10. Three dimensional isosurface plot of mass fraction of oxygen at 873 K.

To study the effect of temperature on the fuel cell cathode the temperature 873, 973, 1073, 1173 and 1273 K were investigated. Since SOFCs have operating temperature between 923–1273 K as shown in TABLE I, investigated temperature is chosen for those values. Fig. 5 - Fig. 19 are shown three dimensional mass fraction of oxygen and electrical potential at temperature 873, 973, 1073, 1173 and 1273 K, respectively. The maximum of mass fraction of oxygen is around 0.144

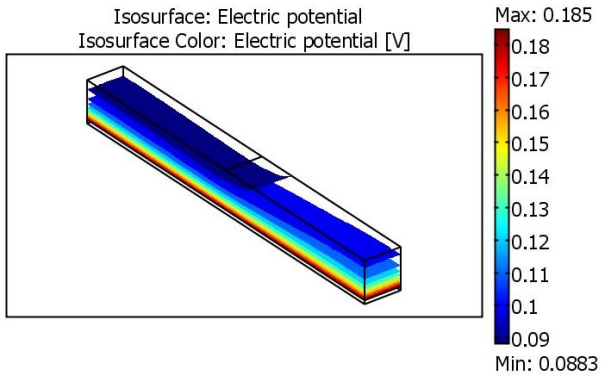

Fig. 11. Three dimensional isosurface plot of electric potential at 873 K.

at all temperature but for the minimum of mass fraction of oxygen depends on temperature. When temperature is increased, the minimum temperature is also increased. The maximum values of electric potential are 0.185, 0.186, 0.187 and 0.188 V. The values have changed very little. On the other hand, the minimum values of electric potential are gradually increased when temperature is increased. The minimum values are 0.088, 0.105, 0.122, and 0.154 V when the temperature is increased from 873 to 1273 K, respectively.

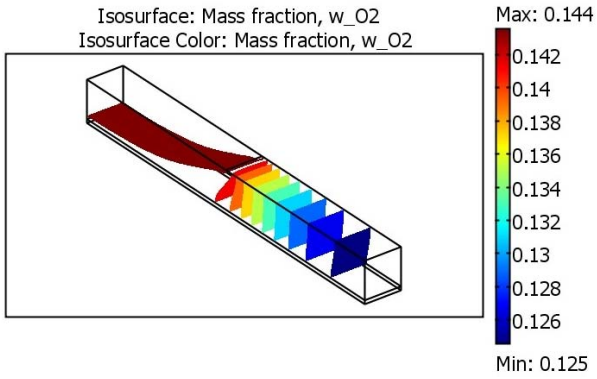

Fig. 12. Three dimensional isosurface plot of mass fraction of oxygen at 973 K.

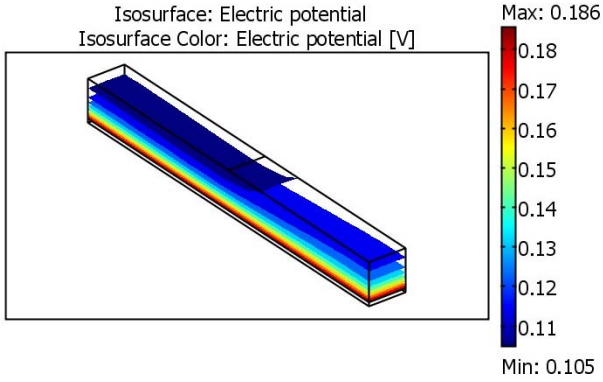

Fig. 13. Three dimensional isosurface plot of electric potential at 973 K.

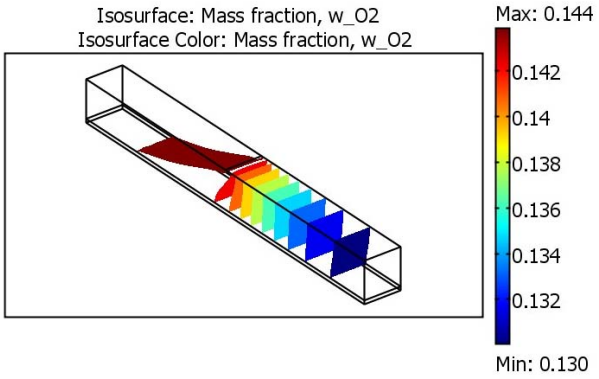

Fig. 14. Three dimensional isosurface plot of mass fraction of oxygen at 1073 K.

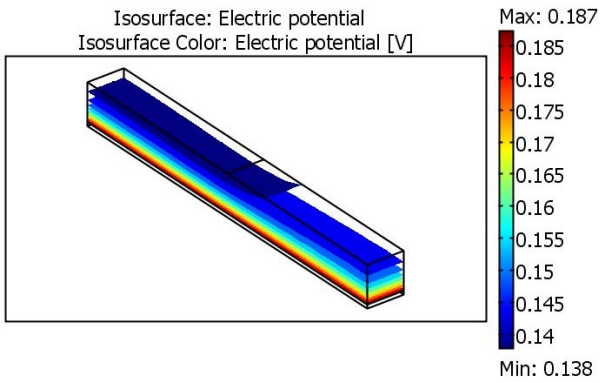

Fig. 17. Three dimensional isosurface plot of electric potential at 1173 K.

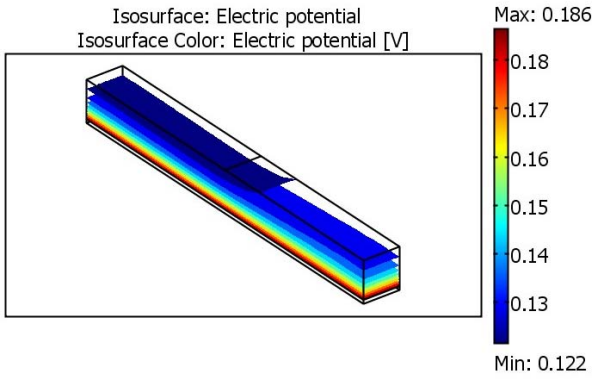

Fig. 15. Three dimensional isosurface plot of electric potential at 1073 K.

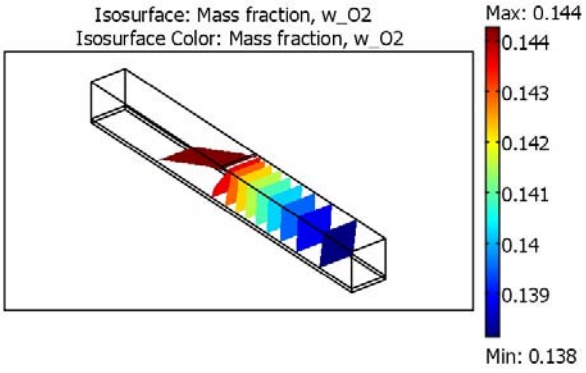

Fig. 18. Three dimensional Isosurface plot of mass fraction of oxygen at 1273 K.

Fig. 20 shows the line plot of electric potential in reactive layer with 5 different temperature. It is clear that electric potential is increased when temperature is increased. Fig. 21 shows the line plot of electric potential in electrolyte layer. It is clear that the pattern is as same as in the reactive layer. The value is between 0.186–0.189 V. The comparison of mass fraction of oxygen is shown in Fig. . As temperature increases, mass fraction is increased in the left hand side of the fuel cell and reach the same maximum value at the right hand side of the fuel cell.

IV. Conclusion

Mathematical models of fuel cells are the system of equations used to described the behavior of the fuel cells. Various mathematical models are used to investigate the performance of various fuel cells. In this study, a mathematical model for fuel cell cathode is investigated. The model is coupled the equations for electron transport, the Maxwell-Stefan equation, and Darcy's law for flow in porous media. The numerical results of the fuel cell cathode are examined using finite

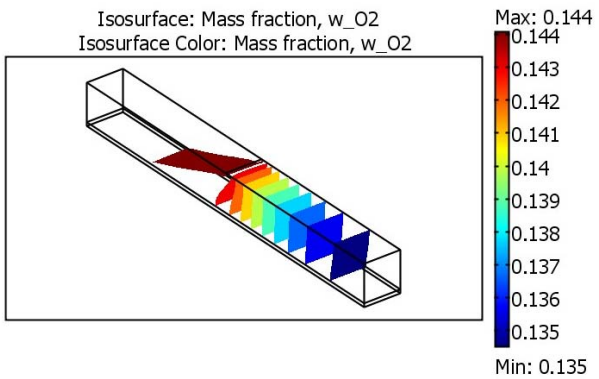

Fig. 16. Isosurface plot of mass fraction of oxygen at 1173 K.

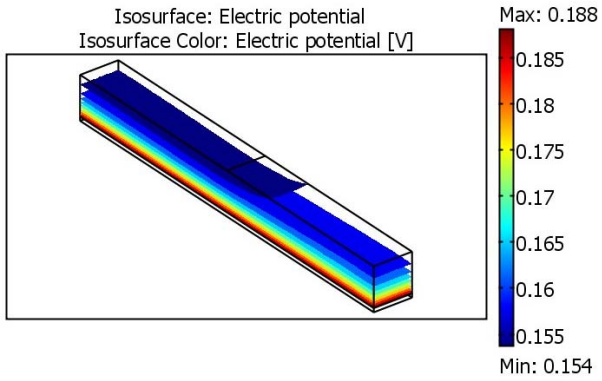

Fig. 19. Three dimensional isosurface plot of electric potential at 1273 K.

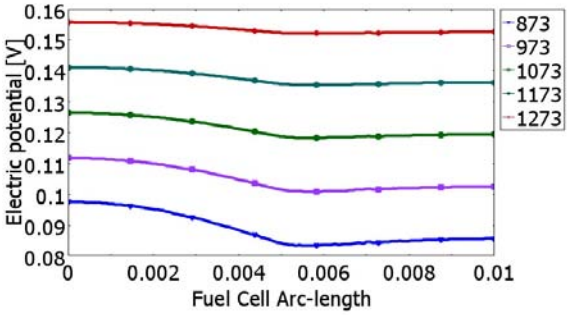

Fig. 20. Line plot of electric potential in reactive layer at temperature 873, 973,1073, 1173, and 1273 K.

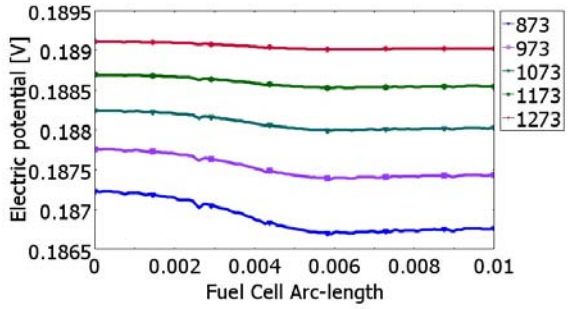

Fig. 21. Line plot of electric potential in electrolyte layer at temperature 873, 973,1073, 1173, and 1273 K.

element method. The mass fraction of oxygen, velocity field, and electric potential are presented. With high temperature, the results indicate that the concentration of total potential drop over the domain, the highest concentration of oxygen is on the right side of the fuel cell, the maximum value of the mass fraction of oxygen is 0.145 and the maximum value of electric potential is in the electrolyte layer. The temperature variation investigation is studied by using five different values which are 873, 973, 1073, 1173, and 1273 K. The higher temperature gives higher electric potential and mass fraction of oxygen. It is showed that the mathematical model is capable to model the high temperature fuel cell cathode.

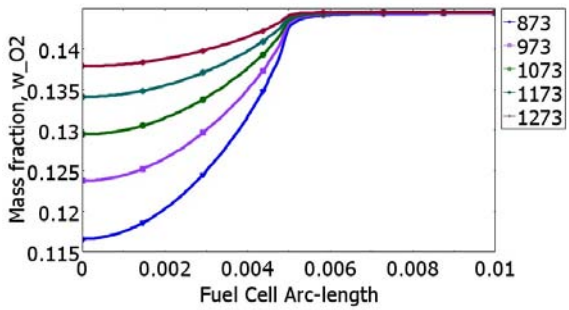

Fig. 22. Line plot of mass fraction of oxygen in reactive layer at temperature 873, 973,1073, 1173, and 1273 K.

ACKNOWLEDGMENT

This research is supported by the Centre of Excellence in Mathematics, the Commission on Higher Education, Thailand. The authors are grateful to Prof. Benchawan Wiwatanapataphee for her helpful suggestions and comments on this paper. The authors would also like to thank the referee for valuable comments on an earlier version of this paper.

REFERENCES

[1] N. Akhtar and P.J.A.M. Kerkhof, *Dynamic behavior of liquid water transport in a tapered channel of a proton exchange membrane fuel cell cathode*, International Journal of Hydrogen Energy **36** (2011), no. 4, 3076 – 3086.

[2] Charalampos Arapatsakos, Dimitrios Christofridis, and Styliani Gkavaki, *The fuel temperature influence on gas emissions when it is used diesel-palm oil mixtures as fuel*, International Journal of Energy **6** (2012), no. 1, 51–64.

[3] Charalampos Arapatsakos, Anastasios Karkanis, Marianthi Moschou, and Ioannis Pantokratoras, *The variation of gas emissions in an otto engine by using different gases as fuel*, International Journal of Energy and Environment **6** (2012), no. 1, 49–56.

[4] J.J. Baschuk and Xianguo Li, *A comprehensive, consisten and systematic mathematical model of pem fuel cells*, Applied Energy **86** (2009), 181–193.

[5] Wei-Hsin Chen, Mu-Rong Lin, Tsung Leo Jiang, and Ming-Hong Chen, *Modeling and simulation of hydrogen generation from hightemperature and low-temperature water gas shift reactions*, International journal of hydrogen energy **33** (2008), 6644–6656.

[6] European commission, *Hydrogen energy and fuel cells: a vison of our future*, Directorate-General for research, 2003.

[7] Orlando Corigliano, Gaetano Florio, and Petronilla Fragiacomo, *Employing solid urban waste in an iir-sofc in cogenerative arrangement*, International Journal of Energy **4** (2010), no. 2, 17–28.

[8] C.Y. Du, X.Q. Cheng, T. Yang, G.P. Yin, and P.F. Shi, *Numerical simulation of the ordered catalyst layer in cathode of proton exchange membrane fuel cells*, Electrochemistry Communications **7** (2005), no. 12, 1411 – 1416.

[9] K Eguchi, H Kojo, T Takeguchi, R Kikuchi, and K Sasaki, *Fuel flexibility in power generation by solid oxide fuel cells*, Solid State Ionics **152153** (2002), no. 0, 411 – 416, ¡ce:title¿PROCEEDINGS OF INTERNATIONAL CONFERENCE ON SOLID STATE IONICS, (MATERIALS AND PROCESSES FOR ENERGY AND ENVIRONMENT), CAIRNS, AUSTRALIA, 8-13 JULY, 2001¡/ce:title¿.

[10] A. Flemming and J. Adamy, *Modeling solid oxide fuel cells using continuous-time recurrent fuzzy systems*, Engineering applications of artificial intelligence **21** (2008), 1289–1300.

[11] M. Garcia-Camprubi, A. Sanchez-Insa, and N. Fueyo, *Multimodal mass transfer in solid-oxide fuel-cells*, Chemical Engineering Science **65** (2010), 1668–1677.

[12] S. Ahmad Hajimolana, M. azlan Hussain, W.M. Ashri Wan daud, M. Soroush, and A. Shamiri, *Mathematical modeling of solid oxide fuel cells: A review*, Renewable and Sustainable Energy Reviews **15** (2011), 1893–1917.

[13] S.A. Hajimolana, M.A. Hussain, W.M.A. Wan Daud, and M.H. Chakrabarti, *Dynamic modelling and sensitivity analysis of a tubular sofc fuelled with nh3 as a possible replacement for h2*, Chemical Engineering Research and Design (2012), no. 0, –.

[14] Thinh X. Ho, Pawel Kosinski, Alex C. Hoffmann, and Arild Vik, *Numerical modeling of solid oxide fuel cells*, Chemical Engineering Science **63** (2008), 5356–5365.

[15] Ta-Jen Huang, Chen-Yi Wu, and Chun-Hsiu Wang, *Fuel processing in direct propane solid oxide fuel cell and carbon dioxide reforming of propane over niysz*, Fuel Processing Technology **92** (2011), no. 8, 1611 – 1616.

[16] M.M. Hussain, X. Li, and I. Dincer, *Mathematical modeling of planar solid oxide fuel cells*, Journal of Power Sources **161** (2006), 1012–1022.

[17] Sadik Kakac, Anchasa Pramuanjaroenkij, and Xiang Yang Zhou, *A review of numerical modeling of solid oxide fuel cells*, International Journal of Hydrogen Energy **32** (2007), 761–786.

[18] Tamer Khatib, Azah Mohamed, M. Mahmoud, and K. Sopian, *Estimating global solar energy using multilayer perception artificial neural network*, International Journal of Energy **6** (2012), no. 1, 25–33.

[19] A. R. Maher and Sadiq Al-Baghdadi, *A cfd study of hygro-thermal stresses distribution in pem fuel cell during regular cell operation*, Renewable Energy **34** (2009), 674–682.

[20] Jose Javier San Martin, Jose Ignacio San Martin, Victor Aperribay, Inigo Javier Oleagordia, Inaki Martin, and Jose M Arrieta, *Technologies of pem fuel cells and their application to led semaphores and lighting systems*, International Journal of Computers **2** (2008), no. 3, 248–258.

[21] G. Nahar and K. Kendall, *Biodiesel formulations as fuel for internally reforming solid oxide fuel cell*, Fuel Processing Technology **92** (2011), no. 7, 1345 – 1354.

[22] Meng Ni, Dennis Y.C. Leung, and Michael K.H. Leung, *Mathematical modeling of ammonia-fed solid oxide fuel cells with different electrolytes*, International Journal of Hydrogen Energy **33** (2008), no. 20, 5765–5772.

[23] _____, *Electrochemical modeling and parametric study of methane fed solid oxide fuel cells*, Energy Conversion and Management **50** (2009), 268–278.

[24] Rapidah Othman, Andrew L. Dicks, and Zhonghua Zhu, *Non precious metal catalysts for the pem fuel cell cathode*, International Journal of Hydrogen Energy **37** (2012), no. 1, 357 – 372, ¡ce:title¿11th China Hydrogen Energy Conference¡/ce:title¿.

[25] Anchasa Pramuanjaroenkij, Sadik Kaka, and Xiang Yang Zhou, *Mathematical analysis of planar solid oxide fuel cells*, International Journal of Hydrogen Energy **33** (2008), no. 10, 2547 – 2565.

[26] Zhigang Qi and Arthur Kaufman, *Low pt loading high performance cathodes for pem fuel cells*, Journal of Power Sources **113** (2003), no. 1, 37 – 43.

[27] Kakac Sadik, Pramuanjaroenki JB Anchasa, and Xiang Yang Zhou, *A review of numerical modeling of solid oxide fuel cells*, International journal of hydrogen energy **32** (2007), 761–786.

[28] Y. Shiratori, T. Oshima, and K. Sasaki, *Feasibility of direct-biogas sofc*, International Jounal of Hydrogen Energy **33** (2008), 6316–6321.

[29] R. Suwanwarangkul, E. Croiset, E. Entchev, S. Charojrochkul, M.D. Pritxker, M.W. Fowler, P.L. Douglas, S. Chewathanakup, and H. Mahaudom, *Experimental and modeling study of solid oxide fuel cell operating with sysgas fuel*, Journal of Power Sources **161** (2006), 308–322.

[30] K. Tseronisa, I. K. Kookosb, and C. Theodoropoulosa, *Modelling mass transport in solid oxide fuel cell anodes: a case for a multidimensional dusty gas-based model*, Chemical Engineering Science **63** (2008), 5626–5638.

[31] Huizhi Wang, Dennis Y.C. Leung, and Jin Xuan, *Modeling of an air cathode for microfluidic fuel cells: Transport and polarization behaviors*, International Journal of Hydrogen Energy **36** (2011), no. 22, 14704 – 14718, ¡ce:title¿Fuel Cell Technologies: FUCETECH 2009¡/ce:title¿.

[32] Qianpu Wang, Datong Song, Titichai Navessin, Steven Holdcroft, and Zhongsheng Liu, *A mathematical model and optimization of the cathode catalyst layer structure in pem fuel cells*, Electrochimica Acta **50** (2004), no. 23, 725 – 730, ¡ce:title¿Polymer Batteries and Fuel Cells:Selection of Papers from First International Conference¡/ce:title¿.

[33] H. Yakabe, T. Ogiwara, M. Hishinuma, and I. Yasuda, *3-d model calculation for planar sofc*, Journal of Power Sources **102** (2001), no. 1-2, 144–154.

[34] Qiangu Yan and Junxiao Wu, *Modeling of single catalyst particle in cathode of pem fuel cells*, Energy Conversion and Management **49** (2008), no. 8, 2425 – 2433.

[35] W.J. Yang, S.K. Park, T.S. Kim, J.H. Kim, J.L. Sohn, and S.T. Ro, *Design performance analysis of pressurized solid oxide fuel cell/gas turbine hybrid systems considering temperature constraints*, Journal of Power Sources **160** (2006), no. 1, 462 – 473.